World Academy of Science, Engineering and Technology
International Journal of Materials and Metallurgical Engineering
Vol:16, No:2, 2022

In-situ LDH Formation of Sodium Aluminate Activated Slag

Tao Liu, Qingliang Yu, H. J. H. Brouwers

***Abstract*—**Among the reaction products in the alkali activated ground granulated blast furnace slag (AAS), the layered double hydroxides (LDHs) have a remarkable capacity of chloride and heavy metal ions absorption. The promotion of LDH phases in the AAS matrix can increase chloride resistance. The objective of this study is that using the different dosages of sodium aluminate to activate slag, consequently, promoting the formation of in-situ LDH. The hydration kinetics of the sodium aluminate activated slag (SAAS) was tested by the isothermal calorimetry. Meanwhile, the reaction products were determined by X-ray diffraction (XRD), thermogravimetric analysis (TGA), and Fourier-transform infrared spectroscopy (FTIR). The sodium hydroxide activated slag is selected as the reference. The results of XRD, TGA, and FTIR showed that the formation of LDH in SAAS is governed by the aluminate dosages.

***Keywords*—**Ground granulated blast furnace slag, sodium aluminate activated slag, in-situ LDH formation, chloride absorption.

I. Introduction

ALKALI activated materials (AAMs) can represent a sustainable alternative to Portland cement in many applications due to its high mechanical property and chemical resistance. The chloride resistance is one of the significant parameters to evaluate the long-term durability of AAMs [1], [2]. Previous studies exhibited that the alkali activated ground granulated blast furnace slag (AAS) had a dense microstructure to resist the chloride penetration [3]. Meanwhile, the layered double hydroxides (LDHs), the secondary reaction products of AAS, have a remarkable capacity for chloride absorption [4]. The external-added LDHs in AAMs showed satisfactory performance towards chloride resistance [5]. However, the costly and complicated synthetic process highly limits the external-added LDHs in AAS to tackle the chloride penetration issue [6]. The promotion of in-situ formatted LDHs is one promising method to enhance the chloride resistance of the AAMs matrix.

The chloride resistance of AAMs is mainly affected by the microstructure (ion transportation) and reaction products (physical absorption and chemical binding) [2]. The dense microstructure and low porosity impede the chloride ion transportation in the AAMs matrix resulting in the high chloride resistance [7]. The formation of gels and crystalline phases influence the evolution of the pore structure [8]. Furthermore, the formation of the gel is controlled by the content of Si-O and Al-O monomers in the pore solution, which is dissolved from the raw materials or provided by the activator [6]. Meanwhile, the formation of some specific crystalline phases, especially LDHs, is influenced by the Mg^{2+} and $Al(OH)_4^-$ in the pore solution [9]. And the $Al(OH)_4^-$ normally comes from solid precursors. Thus, the silicate and aluminate contents are important to the reaction products, which influences the evolution of the pore structure, further influences the chloride resistance of the matrix.

Furthermore, the promotion LDHs formation in the matrix is elucidated by the potentially enhanced chloride binding capacity [4]. Enabling the preferential formation of LDHs ultimately improves the chloride resistance of the AAMs matrix. Liu et al. [10] investigated the effect of MgO, Mg-Al-NO_3-LDH, and CLDH on the chloride resistance of AAMs. The synthetic Mg-Al-NO_3-LDH improved the microstructure and highly reduced chloride penetration in the AAMs matrix. Yang et al. [4] reported that the chloride binding of LDHs was mainly contributed by the surface absorption. The minority of chloride binding was attributed to the ions exchange of LDHs. As mentioned, the cation layer of LDHs is Mg and Al. The concentration of aluminate is a significant factor controlling the crystallization of LDHs. Thereby, the sodium aluminate fits the activation of slag providing extra $Al(OH)_4^-$ in the pore solution. The previous study [11] reported that sodium aluminate activation could build comparable strength at the late curing ages. But the feasibility of sodium aluminate activation to promote the LDHs formation remains poorly understood.

This study aims to investigate the effect of the dosage on the sodium aluminate activation of slag. The reaction heat flow was determined to study the reaction kinetics. Also, the reaction products were identified. The chloride absorption test was performed to evaluate the corresponding chloride absorption property.

II. Experiment

A. Materials

Ground granulated blast-furnace slag (GGBS) was used in this study. The chemical compositions were determined by X-ray fluorescence (XRF), as shown in Table I. The crystalline structure was determined by X-ray diffraction, as shown in Fig. 1. The particle size distribution (PSD) of the powder feedstocks was determined by laser granulometry, using a Master Sizer laser granulometry with an open measuring cell. The preparation of the powders was done by wet dispersion in

Tao Liu is with the Eindhoven University of Technology, Netherlands (phone: +31 0644140823, e-mail: t.liu1@tue.nl).

Qingliang Yu and H. J. H. Brouwers are with the Eindhoven University of Technology, Eindhoven, 5600 MB, Netherlands (e-mail: q.yu.1@tue.nl, jos.brouwers@tue.nl).

deionized water. The particle size distribution is shown inFig. 1, with the median particle size (d_{50}) of 18 μm.

TABLE I
CHEMICAL COMPOSITIONS AND PHYSICAL PROPERTIES OF GGBS

Chemical composition	GGBS (wt. %)
MgO	8.4
Al_2O_3	13.1
SiO_2	31.1
SO_3	3
K_2O	0.4
CaO	41.6
TiO_2	1.6
MnO	0.3
Fe_2O_3	0.5
LOI* (1000□)	1.343
Particle density (g/cm^3)	2.952
BET Specific surface area (m^2/g)	0.347

*LOI = loss on ignition at 1000 □

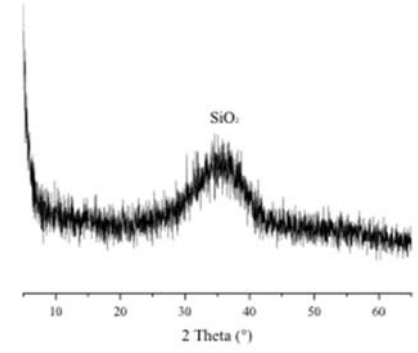

(a)

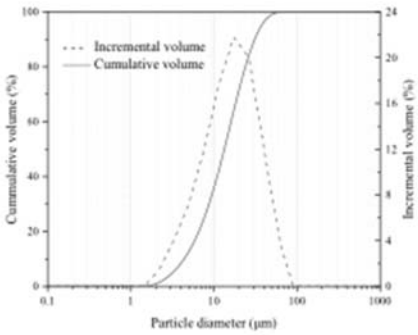

(b)

Fig. 1 (a) X-ray diffractogram of GGBS; (b) Particle size distribution of GGBS

B. Sample Preparations

The GGBS was activated by sodium hydroxides and sodium aluminate solutions, respectively (see the sample IDs in 0). The starting raw materials were mixed with the designed proportion in a Hobart mixer following the preparation procedure suggested by EN 196-1 [12]. The pastes were cast in the Ø 45 mm × 55 mm cylindrical plastic mold followed by vibration. All the pastes were sealed and cured at the ambient temperature until the specified curing ages.

TABLE II
FORMULATION OF THE PASTES

Sample	W/B ratio	$NaAlO_2$ (wt. %)	NaOH (wt. %)	Na_2O (wt. %)	GGBS (wt. %)
NaAl3	0.4	3	-	1.13	100
NaAl4	0.4	4	-	1.51	
NaAl5	0.4	5	-	1.88	
NaAl6	0.4	6	-	2.27	
NaOH-Ref	0.4	-	5	3.88	

C. Testing Methods

1. Isothermal Calorimetry

The heat flow of the samples activated by different activators was measured by isothermal calorimetry set at 20□ (TAM AIR Calorimetry). The results were normalized by the mass of the solids.

2. X-Ray Diffractometry

X-ray diffractometry (XRD) was performed by using a Bruker D4 Phaser instrument with Co-K_α radiation (40 kV, 30 mA). The pressed powdered specimens were measured with a step size of 0.05° and a counting time of 1 s/step, from 10° to 60° 2θ.

3. Thermogravimetry

The thermogravimetric (TG) test was conducted by using an STA 449 F1 instrument, at a heating rate of 10□/min, to samples of ≈ 100 mg. Experiments were carried out from 40□ to 1000□, and during the test process, N_2 was used as the carrier gas. Before the test, the pastes were ground to powder. Then the powder samples were immersed in 2-propanol for 24 hours to stop the hydration process. Subsequently, the powder samples were dried in an oven at 60□ for 3 days to remove the remaining free water and stored in the sealed plastic bag.

4. Fourier-Transform Infrared Spectroscopy

Fourier-transform infrared spectroscopy (FTIR) analysis was performed using a Varian 670-IR spectrometer with a wavelength range of 400 cm^{-1} to 4000 cm^{-1} with a resolution of 1 cm^{-1}.

5. Chloride Leaching-Absorption Test

An accelerated chloride leaching-absorption test was used to study the chloride absorption of SAAS pastes. The paste samples were performed with 3.55 mg/L NaCl solution on material with a particle size < 4 mm and at the liquid to solid ratio10/l (EN 12457 part 2 [13]). In the one-stage batch leaching test the contact time between the solid material and the leachate was 24 hours. After the leaching test, the eluate was filtrated through a 0.45 μm filter and analyzed for chloride ions by using the Ion Chromatography (IC).

III. RESULTS AND DISCUSSION

A. Reaction Kinetics

Previous studies reported the reaction heat flow of alkali activated slag intensively, the induction period finished within the initial 2 days. According to reference [14], the acceleration

and deceleration periods were associated with a high heat release from the nucleation, growth, and precipitation of the reaction products. In this study, different weight percentages of $NaAlO_2$ were applied in the GGBS matrix as the activator, to investigate the role of $NaAlO_2$ in terms of reaction kinetics using isothermal calorimetry.

Fig. 2 presents the normalized reaction heat flow, time to the first reaction peak (TTFRP), and the peak height of pastes. A distinctive difference between samples can be observed. Generally, the higher $NaAlO_2$ content in the activated matrix, the shorter TTFRP, and the higher reaction peak can be obtained. The NaOH-Ref shows the shortest TTFRP and highest peak height. It is due to the relatively higher alkalinity of the paste matrix. While the TTFRPs of SAAS are distinctively longer than that of sodium hydroxides activated slag. Simultaneously, the peak heights of SAAS are notably lower than that of sodium hydroxides activated slag. To discuss it further, the TTFRP of sodium aluminate activated slag presents a decreasing trend with higher content of sodium aluminate. On the one hand, the higher content of sodium aluminate provides extra equivalent Na_2O, namely, higher alkalinity. On the other hand, more $Al(OH)_4^-$ from the sodium aluminate activator in the pore solution accelerates the reaction process to some extent. Thus, the TTFRP decreases with the higher $NaAlO_2$ content. Furthermore, the extra $Al(OH)_4^-$ promotes the early reaction process resulting in increased peak height. It might be noted that the NaAl3 exhibits an extremely low peak height. It is owing to the low reaction degree in line with the thermogravimetric analysis in part 2 of Section III (B) . Generally, the sodium aluminate shows the slow initial reaction kinetics compared to the sodium hydroxides activated slag.

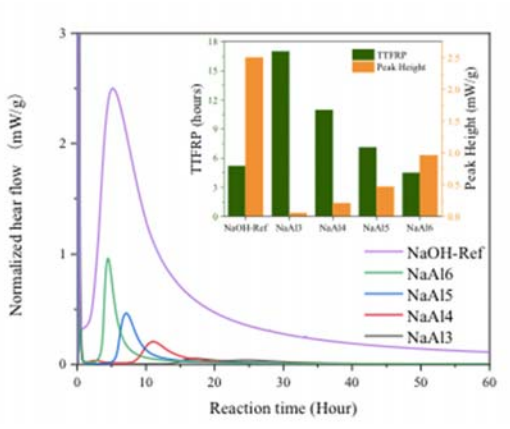

Fig. 2 Normalized reaction heat flow

B. *Reaction Products*

1. X-Ray Diffraction

Fig. 3 shows the XRD patterns of sodium aluminate and sodium hydroxides activated slag at 28 days. The following phases are identified: Calcium Silicate Hydrate (C-S-H) (Tobermorite, JCPDS-ICDD 00-006-0010), Calcium Aluminum Oxide Carbonate Hydroxide Hydrate (Hemicarbonaluminate (Hc), JCPDS-ICDD 00-041-0221), Zeolite LTA (JCPDS-ICDD 01-089-8015), Hydrotalcite (JCPDS-ICDD 00-041-1428), and Calcite (JCPDS-ICDD 01-072-1214).

The primary reaction products of NaOH-Ref are C-S-H, hydrotalcite, and Hc, which is in line with the previous study. However, the hydrotalcite, Hc, and Zeolite LTA are the primary reaction products in the NaAl6. The peak of C-S-H is not obvious. It is associated with the very low alkalinity of the matrix. Besides, the intensities of hydrotalcite, Hc, and Zeolite LTA become stronger with the increasing content of sodium aluminate. The higher pH of the pore solution in SAAS is sufficient to dissolve the slag particles to generate hydrotalcite, Hc, and Zeolite LTA. It should be noted that the formation of Zeolite LTA is due to the extra $Al(OH)_4^-$ in the pore solution [15]. Meanwhile, the intensity of calcite shows a decreasing trend with higher sodium aluminate incorporation. The cause of it may be that the dissolved Ca^{2+} reacts with $Al(OH)_4^-$, CO_3^{2-}, and OH^- to form Hc. Less Ca^{2+} binds with CO_3^{2-} transferring directly to calcite.

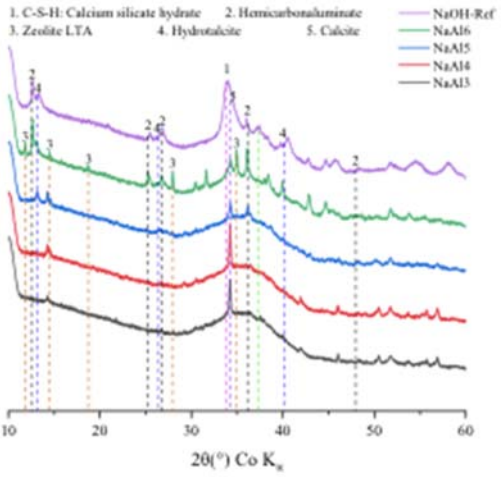

Fig. 3 XRD patterns of sodium aluminate activated slag at 28 days

2. Thermogravimetric Analysis

Fig. 4 illustrates the Thermogravimetry (TG) curves and Differential thermogravimetry (DTG) curves of the paste samples at 28 days. The first largest peak of NaOH-Ref in Fig. 4 (a) is from the thermal decomposition of C-S-H and Hc ranging from 40□ to 300□. It is mainly from the bound water of C-S-H [16]. The predominated phase of NaOH-Ref is C-S-H. Meanwhile, the first peak of hydrotalcite is covered between 150□ to 250□ [9]. The second-largest peak is attributed to the second-step decomposition of hydrotalcite ranging from 300□ to 450□ [9]. Likewise, Fig. 4 (a) illustrates that NaAl6 has a distinctive decomposition of C-(A)-S-H. The extra $Al(OH)_4^-$ has a high possibility involving in the silicate chain. The decompositions of Hc, Zeolite LTA are covered by the largest peak of DTG [17], [18]. At the same time, the first-step decomposition of the hydrotalcite is also overlapped by this peak. In addition, it could be seen that the peak intensity of NaAl3, NaAl4, and NaAl5 is relatively low than that of NaAl6 and NaOH-Ref. It is owing to the low alkalinity of the matrix

resulting in the lower reaction degree. Thus, the decompositions of Zeolite LTA and Hc are the predominated phases rather than C-S-H in NaAl3, NaAl4, and NaAl5. Besides, the calcite becomes the stabler form with the lower content of sodium aluminate. Since the peak around 550□ is the polymorphs type of calcite, while the peak around 700□ is mainly from the crystalline form of calcite [19].

The highest mass loss in Fig. 4 (b) is associated with the C-S-H in NaOH-Ref. It is easy to find that the NaAl6 also exhibits a large amounts of gels formation than other SAAS samples. Simultaneously, the hydrotalcite content of NaAl6 is higher than other SAAS samples. The cause of it is the low alkalinity of the activator. The 6 wt.% of the sodium aluminate is the minimum content to activate the GGBS since it provides a very low pH environment dissolving the raw materials. To make the reaction degree of sodium aluminate activation comparable with the sodium hydroxides, a higher content of equivalent Na_2O is necessary.

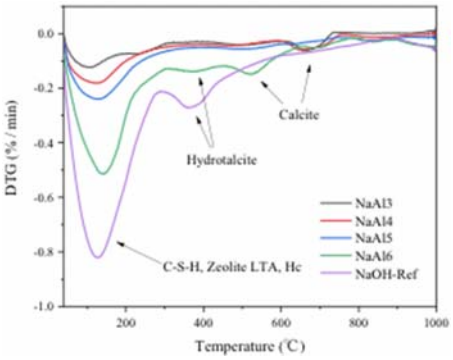

(a)

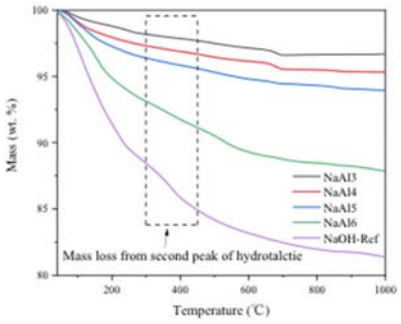

(b)

Fig. 4 Paste samples at 28 days (a) Differential thermogravimetry (DTG) curves; (b) Thermogravimetry (TG) curves.

3. Fourier-Transform Infrared Spectroscopy

Fig. 5 exhibits the FTIR spectrum of pastes at 28 days. It is clear to see that the peak of Si-O tetrahedron in NaOH-Ref and NaAl6 is located at 951 cm^{-1}, which is associated with the geopolymerization process in the activated system. The Si-O bonds are attributed to silicate chains in C-S-H, C-A-S-H, or N-A-S-H gels. However, no obvious peak at this position is shown in the NaAl3, NaAl4, and NaAl5. It represents that few Si-O tetrahedra in the activated systems result in a low reaction degree. Simultaneously, the O-H bands NaOH-Ref and NaAl6 are associated with bound water in the -S-H, C-A-S-H, or N-A-S-H gels. While the no obvious peaks are shown in the NaAl3, NaAl4, and NaAl5, either. Meanwhile, the vibrations at 670, 1397, and 1484 are from the carbonate groups. It is reflected by the calcite and its polymorphs type. Overall, the Si-O, O-H, and C-O bonds are in line with results in parts 1 and 2 in Section III (B).

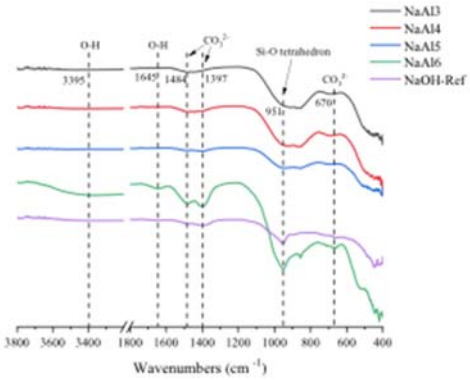

Fig. 5 FTIR spectrum of pastes at 28 days

C. Chloride Absorption

Fig. 6 (a) illustrates the chloride ions concentration in the remaining solution after 24-24 leaching of the SAAS samples. The original NaCl solution is 3.55 mg/L. The normalized chloride absorption by the SAAS samples is presented in Fig. 6 (b).

It can be seen that the NaOH-Ref shows the lowest remaining chloride ions concentration and the highest absorption. Similarly, the NaAl6 shows the second-lowest remaining chloride ions concentration and the second-highest absorption among the samples. It is due to the large amount of C-S-H gels driving by the relatively high reaction degree. Meanwhile, the hydrotalcite in NaOH-Ref and NaAl6 contributes to chloride absorption as well. Since the chloride ions can be absorbed on the surface of hydrotalcite, also it can be exchanged into the interlayer of hydrotalcite. Similar chloride absorptions are reflected in NaAl3, NaAl4, and NaAl5. The chloride absorption may be attributed to the small amount of zeolite in the matrix. Overall, the contents of gels and hydrotalcite are the dominant contribution in terms of chloride absorption.

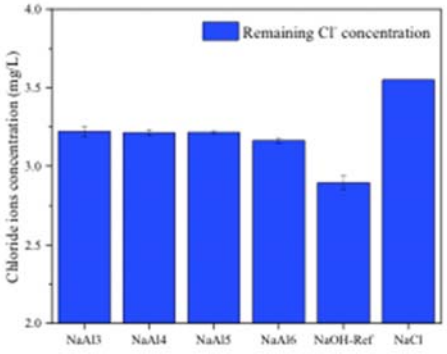

(a)

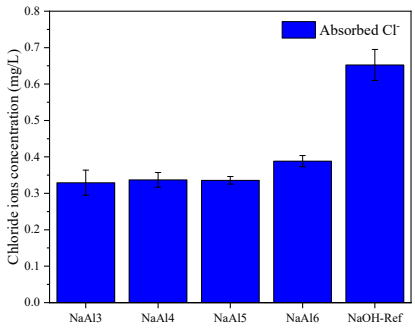

(b)

Fig. 6 Chloride absorption

IV. Conclusions

This study aims to use the different dosages of sodium aluminate to activate slag, consequently, achieving the formation of in-situ LDHs. The results show that the sodium aluminate activator features slow initial reaction kinetics due to the low alkalinity. Meanwhile, the hydrotalcite is observed in the sodium aluminate activated matrix. The following conclusions can be drawn:

- The sodium aluminate activated slag achieves the in-situ formation of LDHs. The LDHs content increases with the higher content of sodium aluminate content.
- 6 wt.% of the sodium aluminate is the minimum content to activate the slag due to its low alkalinity.
- The chloride absorption of SAAS is improved by the higher sodium aluminate content.

References

[1] J. Zhang, C. Shi, Z. Zhang, Z. Ou, Durability of alkali-activated materials in aggressive environments: A review on recent studies, Constr. Build. Mater. 152 (2017) 598–613. doi:10.1016/j.conbuildmat.2017.07.027.

[2] J. Osio-Norgaard, J. P. Gevaudan, W. V. Srubar, A review of chloride transport in alkali-activated cement paste, mortar, and concrete, Constr. Build. Mater. 186 (2018) 191–206. doi:10.1016/j.conbuildmat.2018.07.119.

[3] P. Chen, B. Ma, H. Tan, X. Liu, T. Zhang, C. Li, Q. Yang, Z. Luo, Utilization of barium slag to improve chloride-binding ability of cement-based material, J. Clean. Prod. 283 (2021). doi:10.1016/j.jclepro.2020.124612.

[4] T. Yang, Z. Zhang, F. Zhang, Y. Gao, Q. Wu, Chloride and heavy metal binding capacities of hydrotalcite-like phases formed in greener one-part sodium carbonate-activated slag cements, J. Clean. Prod. 253 (2020). doi:10.1016/j.jclepro.2020.120047.

[5] T. Liu, Y. Chen, Q. Yu, J. Fan, H. J. H. Brouwers, Effect of MgO, Mg-Al-NO3 LDH and calcined LDH-CO3 on chloride resistance of alkali activated fly ash and slag blends, Constr. Build. Mater. 250 (2020). doi:10.1016/j.conbuildmat.2020.118865.

[6] T. Liu, Q. Yu, H. J. H. Brouwers, In-situ formation of layered double hydroxides (LDHs) in sodium aluminate activated slag: The role of Al-O tetrahedra, Cem. Concr. Res. 153 (2022) 106697. doi:10.1016/j.cemconres.2021.106697.

[7] A. A. Ramezanianpour, V. M. Malhotra, Effect of curing on the compressive strength, resistance to chloride-ion penetration and porosity of concretes incorporating slag, fly ash or silica fume, Cem. Concr. Compos. 17 (1995) 125–133. doi:10.1016/0958-9465(95)00005-W.

[8] Z. Zhang, Y. Zhu, H. Zhu, Y. Zhang, J. L. Provis, H. Wang, Effect of drying procedures on pore structure and phase evolution of alkali-activated cements, Cem. Concr. Compos. 96 (2019) 194–203. doi:10.1016/j.cemconcomp.2018.12.003.

[9] C. Forano, U. Costantino, V. Prévot, C. T. Gueho, Layered double hydroxides (LDH), Dev. Clay Sci. 5 (2013) 745–782. doi:10.1016/B978-0-08-098258-8.00025-0.

[10] T. Liu, Y. Chen, Q. Yu, J. Fan, H. J. H. Brouwers, Effect of MgO, Mg-Al-NO3 LDH and Calcined LDH-CO3 on chloride resistance of alkali activated fly ash and slag blends, Constr. Build. Mater. 250 (2020) 118865. doi:10.1016/j.conbuildmat.2020.118865.

[11] J. Yliniemi, B. Walkley, J. L. Provis, P. Kinnunen, M. Illikainen, Influence of activator type on reaction kinetics, setting time, and compressive strength of alkali-activated mineral wools, J. Therm. Anal. Calorim. 144 (2021) 1129–1138. doi:10.1007/s10973-020-09651-6.

[12] EN 196-1, En 196-1, (2005) 1–33.

[13] BS EN 12457-2, Characterisation of Waste - Leaching - Compliance Test for Leaching of Granular Waste Materials and Sludges - Part 2: One stage batch test at a liquid to solid ratio of 10 l/kg for materials with particle size below 4 mm (without or with size reduction), BSI Stand. Publ. 3 (2014) 30.

[14] X. Gao, Q.L. Yu, A. Lazaro, H. J. H. Brouwers, Investigation on a green olivine nano-silica source based activator in alkali activated slag-fly ash blends: Reaction kinetics, gel structure and carbon footprint, Cem. Concr. Res. 100 (2017) 129–139. doi:10.1016/j.cemconres.2017.06.007.

[15] Z. Shi, B. Ma, B. Lothenbach, Effect of Al on the formation and structure of alkali-silica reaction products, Cem. Concr. Res. 140 (2021). doi:10.1016/j.cemconres.2020.106311.

[16] O. Burciaga-Díaz, I. Betancourt-Castillo, Characterization of novel blast-furnace slag cement pastes and mortars activated with a reactive mixture of MgO-NaOH, Cem. Concr. Res. 105 (2018) 54–63. doi:10.1016/j.cemconres.2018.01.002.

[17] S. Berger, C. C. D. Coumes, P. Le Bescop, D. Damidot, Influence of a thermal cycle at early age on the hydration of calcium sulphoaluminate cements with variable gypsum contents, Cem. Concr. Res. 41 (2011) 149–160. doi:10.1016/j.cemconres.2010.10.001.

[18] N. M. Musyoka, L. F. Petrik, E. Hums, A. Kuhnt, W. Schwieger, Thermal stability studies of zeolites A and X synthesized from South African coal fly ash, Res. Chem. Intermed. 41 (2015) 575–582. doi:10.1007/s11164-013-1211-3.

[19] E. R. McCaslin, C. E. White, A parametric study of accelerated carbonation in alkali-activated slag, Cem. Concr. Res. 145 (2021). doi:10.1016/j.cemconres.2021.106454.